Operational modal analysis on a lighthouse structure subjected to ice actions

Nord, Torodd S.; Kvåle, Knut Andreas; Petersen, Oyvind W.; Bjerkås, Morten; Lourens, Eliz Mari

DOI
10.1016/j.proeng.2017.09.268

Publication date
2017

Document Version
Final published version

Published in
X International Conference on Structural Dynamics, EURODYN 2017

Available online at www.sciencedirect.com

ScienceDirect

Procedia Engineering 199 (2017) 1014–1019

Procedia Engineering

www.elsevier.com/locate/procedia

X International Conference on Structural Dynamics, EURODYN 2017

Operational modal analysis on a lighthouse structure subjected to ice actions

Torodd S. Nord[a]*, Knut Andreas Kvåle[b], Øyvind W. Petersen[b], Morten Bjerkås[a], Eliz-Mari Lourens[c]

[a]*Sustainable Arctic Marine and Coastal Technology (SAMCoT), Faculty of Engineering Science and Tecnhology, NTNU, 7491 Trondheim, Norway*

[b]*Department of Structural Engineering, Faculty of Engineering Science and Technology, NTNU, 7491 Trondheim, Norway*

[c]*Faculty of Civil Engineering and Geosciences, Delft University of Technology, the Netherlands.*

Abstract

The sea ice interaction with a structure may cause system changes and affect the feasibility of common approaches to track modal parameters. In this paper, a covariance-driven stochastic subspace identification method is used to identify the natural frequencies from 190 time series of ice actions against a lighthouse structure. The results are sorted into groups defined by the observed ice conditions and governing ice failure mechanisms during the ice-structure interaction. The identified natural frequencies vary substantially within each individual group and between the groups. Recordings with flexural failures and a north-south ice-drift direction consistently rendered the same identified frequencies, whereas crushing seemed to create large amounts of variability in the identified frequencies. The results show the need for more high-fidelity data to assess whether modern system identification methods can be used to monitor system changes and support decision-making for operations of structures in ice-infested waters, such as offshore wind structures.

Peer-review under responsibility of the organizing committee of EURODYN 2017.

Keywords: System identification; Operational modal analysis; Ice-structure interaction

1. Introduction

Ice actions on slender offshore structures have resulted in numerous structural failures in the Baltic Sea [1].

* Corresponding author. Tel.: +47 73594655; fax: +47 73594655.
E-mail address: torodd.nord@ntnu.no

1877-7058
Peer-review under responsibility of the organizing committee of EURODYN 2017.
10.1016/j.proeng.2017.09.268

Several measurement campaigns conducted to quantify the ice forces and resulting responses supported quantitatively the development of international guidelines for the design of Arctic infrastructure, such as ISO/FDIS 19906 [2]. The measurement campaigns on Arctic offshore structures were mostly conducted to better understand ice forces. Several techniques and sensors have been developed by the ice research community to measure ice forces [3], alongside the development of models to predict ice loads and structural responses [4].

System identification is an immature discipline in the context of Arctic offshore structures. Bjerkås [5] used wavelet transforms to study the synchronization of local forces on the Norströmsgrund lighthouse. Londoño [6] performed operational modal analysis (OMA) using time series governed by ambient loading from the wind, traffic, currents and ice as part of a structural health monitoring assessment on the massive Confederation Bridge in Canada. Light ice conditions were intentionally selected for the system identification, as it was stated that the ice conditions themselves may alter the system. Londoño made no further attempts to investigate the system changes caused by the severity of the ice conditions. It is thus unknown to what extent the size of the structure relative to the size of the ice features causes system changes, e.g. changes in the natural frequency, damping and mode shapes, or the introduction of nonlinearities. It is also unknown for which ice conditions the true modal properties can be identified and when the underlying assumptions of the applied algorithms are violated the most. Because the ice forces are sometimes measurable, combined deterministic-stochastic methods may also be applied. The deterministic input can then be described by the measured ice forces, whereas the remaining forces from the wind (and unmeasured ice forces) may be described by the stochastic terms. In several other civil engineering applications, the deterministic force is small compared to the ambient forces. For structures in ice-infested waters, the ice forces are usually governing.

In this paper, we demonstrate the influence of different ice conditions on the identified frequencies for 190 time series of ice-structure interactions on a lighthouse structure. The main contributing source of excitation is the ice forces, and the time series are sorted into groups defined by the observed ice conditions, which enables us to study for which ice conditions the identified system poles significantly change. The time series are carefully selected from the STRICE data-set [7], one of the largest and most important data-sets used in the development of the ISO 19906 design code for Arctic offshore structures. The OMA is conducted with a covariance-driven stochastic subspace method (Cov-SSI) in conjunction with an automatic routine to select the system poles. First, we present the methodology, the measurement setup and the governing ice failure types. Second, the identified modal frequencies are compared for the different ice failure types.

2. Subspace system identification

2.1. State-space models and system identification

A stochastic discrete-time state-space model of a structure can be described as follows:

$$\{z_{k+1}\} = [A]\{z_k\} + \{w_k\} \tag{1}$$

$$\{y_k\} = [C]\{z_k\} + \{v_k\} \tag{2}$$

Here $\{z_k\}$ is the state vector, $\{y_k\}$ is the output vector, $\{w_k\}$ is the process noise, $\{v_k\}$ is the measurement noise, and k is the discrete time increment number. The matrices $[A]$, and $[C]$ are the state matrix and the output influence matrix, respectively, which can be obtained using operational modal analysis. Herein, a covariance-driven stochastic subspace (Cov-SSI) algorithm [8, 9] is used to identify $[A]$ and $[C]$, from which the modal frequencies, damping and mode shapes are obtained.

2.2. Stabilization criteria and pole selection

After the Cov-SSI rendered the state matrix $[A]$, stabilization criteria are used as a means to distinguish between physical and spurious modal estimates. At a certain order n^* with corresponding poles m^*, the stabilization level $\sigma = 1, 2, ..., s$ defines a range in preceding orders, $n = n^* - \sigma$, from which the corresponding poles m are compared with all poles in m^*. The routine needs a modal indicator that suggests which pole in m^* coincides with a pole in m. The modal indicator is defined as the difference in angular natural frequency between the poles in m^* and m such

that $\Delta\omega_{m^*,m} = \omega_{m^*} - \omega_m$. The stability of a pole at order n^* is evaluated by means of the tolerance deviances in the frequency, damping and MAC values between the poles in m^* and m , for all orders $n = n^* - \sigma$,

$$|f_{n^*,m^*} - f_{n,m}|/f_{n^*,m^*} \le C_f, \quad |\xi_{n^*,m^*} - \xi_{n,m}|/\xi_{n^*,m^*} \le C_\xi, \quad \frac{|\{\phi_{n^*,m^*}\}^T\{\bar{\phi}_{n,m}\}|}{\{\phi_{n^*,m^*}\}^T\{\bar{\phi}_{n^*,m^*}\}\cdot\{\phi_{n,m}\}^T\{\bar{\phi}_{n,m}\}} \le C_{MAC} \quad (3)$$

where the deviance values are $C_f = 0.01$, $C_\xi = 0.05$, and $C_{MAC} = 0.95$ and $\bar{\phi}_{n,m}$ is the complex conjugate of $\phi_{n,m}$. A pole at order n^* is deemed stable if it fulfills Eq. (3) for a pole at each order $n = n^* - \sigma$ up to the chosen stability level s . A stability plot is provided in Fig. 2c, where an automatic selection routine (section 4.2) has highlighted and numbered the identified modes for a particular data time series. The reader is referred to [10] for details on the selection of stability levels and their influence on the stabilization plot.

3. Ice-structure interaction

3.1. Ice failure mechanisms

Six types of ice-structure interaction against vertically-faced structures are considered in this paper, and illustrations of these are displayed in Fig. 1. It is recommended to read Jordaan [11] for an overview of the mechanics of ice-structure interaction and Kärnä and Jochmann [7] for descriptions of the observed failure types against the Norströmsgrund lighthouse. Continuous crushing (Fig. 1a) is governed by the non-simultaneous occurrence of so-called high-pressure zones across the ice-structure interface. The bending type of flexural failure is often initiated by a circumferential crack followed by radial cracks (Fig. 1b). Splitting failures (Fig. 1c) are usually observed when the interacting ice sheet has low lateral confinement. The buckling type (Fig. 1d) of flexural failure is governed by a build-up of curvature in the ice sheet. Winds and waves as well as ice management can generate fields of broken ice (Fig. 1 e) that cause small impacts from floes of various sizes onto the face of the structure. The floes split and pass around the structure, while wind and wave actions contribute significantly to the total force. The last interaction type is creep, in which the ice floe simply rests against the structure. The frequency contents of the ice forces vary substantially between the individual failure types but also within the same type of failure with different environmental parameters. Examples of measured ice forces from crushing failure and bending failure are displayed in Fig. 2b. It is undoubtedly important to assess the degree to which we violate the assumption of a white noise input for the Cov-SSI. This is, however, an ongoing research topic and lies outside the scope of this paper.

In this paper, no distinction is made between the different types of ice, e.g. level ice, rafted ice or ice ridges. This means that e.g. crushing ice failure can be caused by any type of ice.

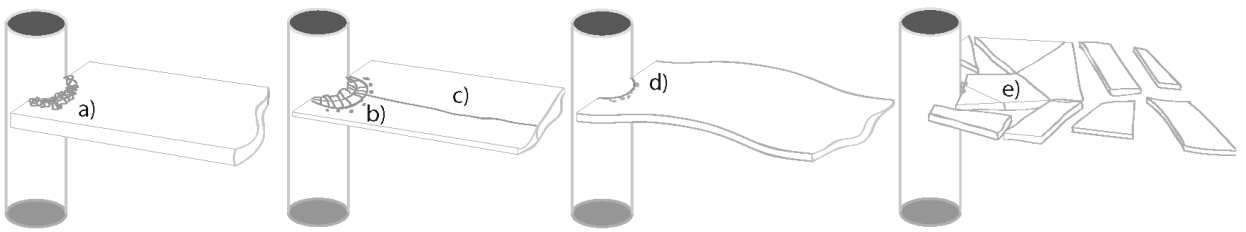

Fig. 1. Interaction types: (a) crushing failure; (b) bending failure; (c) splitting failure; (d) buckling failure; (e) pushing floes.

3.2. Measurements of ice-structure interactions 2001-2003 at the Norströmsgrund lighthouse

The Norströmsgrund lighthouse is located in the Gulf of Bothnia, 60 km southeast of the city of Luleå, Sweden. The structural responses, ice forces, ice thicknesses, air temperatures, wind speeds, wind directions and ice conditions

during the winter seasons from 1999 to 2003 were monitored in the measurement projects LOLEIF (LOw LEvel Ice Forces) [12] and STRICE (STRuctures in ICE) [7]. The gravity-based concrete structure is stiffened by eight concrete bulkheads and a 0.7m thick concrete foundation plate that rests on cement-grouted crushed stones and morainic soil. Nine panels were installed at the mean water level to measure the ice forces [12], covering the outer perimeter from 0 to 162°. Four acceleration channels (Shaevitz SB) and four inclinometer channels (Schaevitz DC inclinometer series and Applied Geomechanics biaxial Model 716-2A) measured the structural accelerations in the north-south and east-west directions and tilts about the same directions, respectively. The accelerometers were located close to the ice-action point at an elevation of +16.5 m and close to the top at an elevation of +37.1 m. A summary of the STRICE project and earlier measurement campaigns can be found in Bjerkås [13].

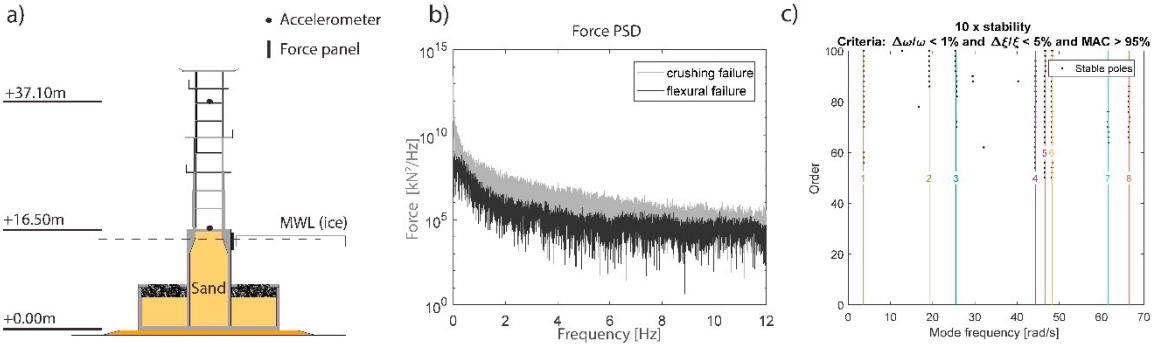

Figure 2. a) Drawing and sensor placement; b) measured ice forces for crushing and flexural failures; c) stabilization plot from one recording.

3.3. Selection of recordings from the STRICE data

Extensive efforts were devoted to the selection of data for this paper, where several criteria had to be fulfilled: the sampling frequency should be at a minimum of 30 Hz, video footage must be available to define the type of failure, and the ice failure should be governed by one of the failure types defined in section 3.1 for a minimum of 4 minutes. The individual data files contain time series of various lengths. They were selected by operators to capture specific types of interactions. Often, one data file has several events of interaction that fulfill the criteria above, and each of these events is from now on referred to as a recording. In total, 190 recordings with lengths of 4 to 10 minutes were selected and further used in this paper, where 83 were crushing, 40 flexural, 22 splitting, 14 floe ice and 31 creep recordings. The accelerations and global forces were resampled to 24 Hz and filtered with a Butterworth high-pass filter with a 0.2 Hz cut-off (-3dB) frequency.

4. Modal identification

4.1. Selection of parameters for the modal identification algorithms

The results depend on the choice of parameters fed to the algorithm, and these choices are explained in this section. The durations of the recordings, T , were chosen based on several considerations. The stationarity of the ice failure process was the most difficult one to fulfill. The governing failure process is intermittently interrupted by other failure mechanisms in most time series, introducing non-stationarity to the signals. It was found that recordings between 4-10 minutes were sufficiently short to obtain recordings of all failure mechanisms. It was always attempted to keep the recordings to 10 minutes, but some had to be shortened because the governing failure process changed.

The number of blockrows, i, is a user defined index that decides the number of time lags for the covariances in the block-Toeplitz matrix for the Cov-SSI. It should ensure sufficiently large time lags in the covariance matrices to represent the lowest frequency of interest in the data. We chose $i = 50$, which with a sampling frequency of 24 Hz

corresponds to a maximum time lag of $\tau = 2 \cdot 50 \cdot \frac{1}{24} = 4.16$ s or a lowest frequency of interest equal to 0.24 Hz. The stabilization level, s, must be chosen alongside the number of blockrows to obtain as little scatter in the stabilization plot as possible. The reader is referred to [10] for figures showing the effects of the chosen s and i, and after several attempts in this study, $s = 10$ seemed to render reasonable stabilization plots. The range of orders was chosen by visual inspection of the stabilization plot and ranges across $n = 2,4,...100$.

4.2. Automatic system identification

After several attempts to manually select the modes from the stability plot, we judged this approach inefficient, providing too little quantitative information on the selection, and it was too much influenced by the analyst. Thus, a simplistic automatic routine was implemented for the selection and numbering of the identified modes. The routine collects all poles that fulfill the stabilization criteria in Eq.(3). The poles are first sorted with increasing corresponding absolute values, and a user-defined frequency slack value, S_f, defines the range in which the poles are collected. From the eigenvectors of the poles in that range, MAC values are calculated between all eigenvectors, and a reference mode is selected as the pole that renders the highest sum of the MAC values. The MAC values between the reference mode and the eigenvectors of the remaining poles in that frequency range (defined by S_f) must lie within a user-defined MAC-slack, S_{MAC} to be further considered. The third acceptance criterion checks whether the poles that fulfill the MAC-slack also fulfill a damping slack, S_ζ. Finally, the selected mode contains the means of the frequency, damping and mode shape. S_f, S_{MAC} and S_ζ were chosen to be 0.02, 0.3 and 0.5, respectively.

An illustration of eight automatically selected modes for a single recording is provided in Fig. 2c. The frequencies corresponding to the eight modes in Fig. 2c appear as a single column of black dots in Fig. 3a, in which the identified frequencies versus the recording number are shown. All types of failure display a scattered plot. Somewhat higher densities of frequencies occur at approximately 1.45, 4.1, 5.0, 7.4 and 10 Hz. Crushing failure (Fig. 3b), which represents the most severe ice condition, gives the most scattered plot in the frequency range 2-4 Hz. The least scatter

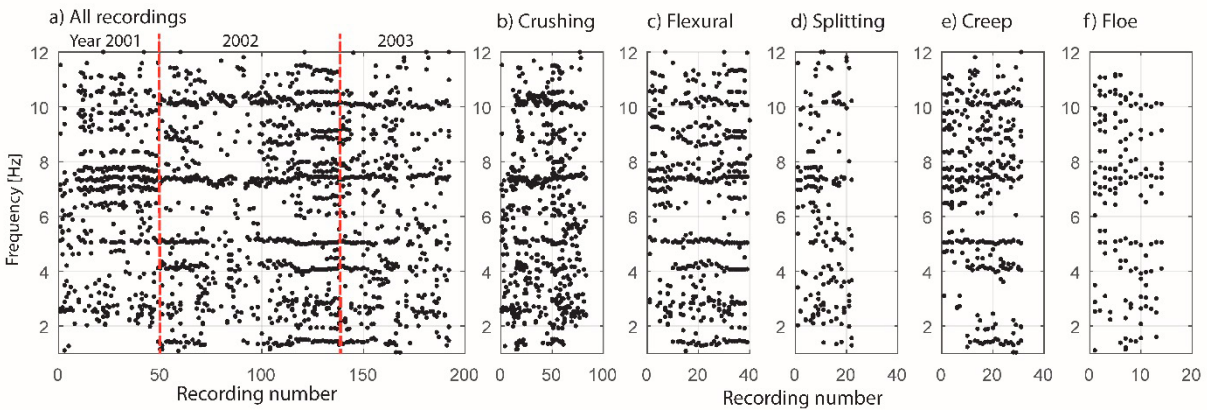

Figure 3. Identified frequencies from the automatically selected poles for different regimes of ice-structure interaction: a) all 190 recordings, with dashed lines separating the years; b) crushing failure; c) flexural failure d) splitting failure; e) creep and f) floe ice.

is found for flexural failures (Fig. 3c) between recordings 31-40, where the ice drift was primarily north-south. Few identified frequencies below 2 Hz were found for the splitting failure (Fig. 3d), and few were found between 2-4 Hz when the ice floe stalls against the structure (creep). The scatter seen for the floe ice interaction (Fig. 3f) was unexpected because as the wind loads become more important, the waves are reflected by ice floes in several directions, and ice-structure contacts have smaller impacts at different locations, all expected to result in the least violation of the input white noise assumption for the Cov-SSI. Attempts were made to test whether the data was inaccurate at low vibration amplitudes by sorting out the recorded events with the highest standard deviations of the acceleration, but no clear indication was found. It is, however, a fact that this is a difficult axisymmetric problem with

an unknown extent of nonlinearity, handled with only a few sensors and an automatic mode selection routine highly dependent on MAC-values. By using a hierarchy clustering method as described in [14], similar results as shown in Fig. 3 were obtained when low importance was assigned to the weights for the MAC-values and clusters with very few poles were discarded. Because the measured forces can be used as inputs in a combined deterministic-stochastic setting, the same automatic modal identification approach was repeated using a combined stochastic-deterministic algorithm [15]. Similar results were found when using the same input parameters as for the Cov-SSI, stabilization criteria and slack values, while the scatter (especially between 2-4 Hz) was reduced. In summary, the large variations of the identified frequencies within the individual types of ice failure made it difficult to find systematic system changes caused by the presence of the ice.

5. Conclusions

In total, 190 carefully selected recordings from a famous ice-structure interaction data set, STRICE, were used for identifying consistent system changes with observed ice conditions. Little consistency between the ice failure processes and identified frequencies was found, and the only clear trend between the identified frequencies and ice conditions was found for recordings in which flexural failures occurred with ice drift in the north-south direction. The inconsistency may be explained by the violation of the underlying assumptions used to derive the applied identification routine, the structural complexity and limited sensor data of uncertain quality. Therefore, the collection and analysis of higher quality full-scale data must continue with the aim of retrieving more useful information about the system changes posed by the different ice conditions, which, in turn, can affect the operation of structures such as offshore wind structures.

Acknowledgements

The authors wish to acknowledge support from the Research Council of Norway through the Centre for Research-based Innovation SAMCoT and support from all SAMCoT partners. The full-scale measurements were funded by the European Commission DG RESEARCH under the Fifth Framework Programme for Research and Development within the Energy, Environment and Sustainable Development (EESD) Programme under the Key Action RTD activities of a generic nature (Contract No. EVG1-CT-2000-00024).

References

[1] M. Bjerkås, T.S. Nord. Ice action on Swedish lighthouses. The 23rd IAHR International symposium on ice. Ann Arbor, Michigan, USA2016.
[2] ISO. ISO/FDIS 19906. 2010. p. 188.
[3] K.R. Croasdale, R. Frederking. Field techniques for ice force measurements. IAHR Symposium on Ice. Iowa City, Iowa, USA1986. p. 443-82.
[4] H. Hendrikse. Ice-induced vibrations of vertically sided offshore structures: Delft University of Technology; 2017.
[5] M. Bjerkås. Wavelet transforms and ice actions on structures. Cold Regions Science and Technology. 2006;44:159-69.
[6] N.A. Londoño. Use of vibration data for structural health monitoring of Bridges. Ottawa: Carleton University; 2006.
[7] T. Kärnä, P. Jochmann. Field observations on failure modes. Port and Ocean Engineering under Arctic Conditions. Trondheim, Norway2003. p. 839-49.
[8] L. Hermans, H. Van Der Auweraer. MODAL TESTING AND ANALYSIS OF STRUCTURES UNDER OPERATIONAL CONDITIONS: INDUSTRIAL APPLICATIONS. Mechanical Systems and Signal Processing. 1999;13:193-216.
[9] C. Rainieri, G. Fabbrocino. Output-only Modal Identification. Operational Modal Analysis of Civil Engineering Structures: An Introduction and Guide for Applications. New York, NY: Springer New York; 2014. p. 103-210.
[10] K.A. Kvåle, O. Øiseth, A. Rönnquist. Operational modal analysis of an end-supported pontoon bridge. Submitted December 2016 to Journal of Engineering Structures 2017.
[11] I.J. Jordaan. Mechanics of ice–structure interaction. Engineering Fracture Mechanics. 2001;68:pp.1923-60.
[12] P. Jochmann, J. Schwarz. Ice force measurements at lighthouse Norströmsgrund- winter 1999, LOLEIF Report No. 5, MAS3-CT-97-0098. Hamburgische shiffbau-versuchsantalt GmbH; 1999. p. 48.
[13] M. Bjerkås. Ice action on offshore structures [PhD]: NTNU, ISBN 82-471-7756-0; 2006.
[14] F. Magalhães, Á. Cunha, E. Caetano. Online automatic identification of the modal parameters of a long span arch bridge. Mechanical Systems and Signal Processing. 2009;23:316-29.
[15] P. Van Overschee, B. De Moor. Subspace identification for linear systems: theory, implementation, applications: Kluwer Academic Publishers, Boston/London/Dordrecht; 1996.